International Journal of Radiation Oncology biology • physics

www.redjournal.org

Biology Contribution

An Assessment of Radiation Doses From Radon Exposures Using a Mouse Model System

Johanna Mirsch, PhD,* Lisa Hintz, MSc,* Andreas Maier, PhD,† Claudia Fournier, PhD,† and Markus Löbrich, PhD*

**Radiation Biology and DNA Repair, Technical University of Darmstadt, Darmstadt, Germany; and †Department of Biophysics, GSI Helmholtzzentrum für Schwerionenforschung, Darmstadt, Germany*

Received Dec 19, 2019. Accepted for publication May 18, 2020.

Background: Radon and its progenies contribute significantly to the natural background radiation and cause several thousands of lung cancer cases per year worldwide. Moreover, patients with chronic inflammatory joint diseases are treated in radon galleries. Due to the complex nature of radon exposure, the doses associated with radon exposures are difficult to assess. Hence, there is a clear need to directly measure dose depositions from radon exposures to provide reliable risk estimates for radiation protection guidelines.

Objectives: We aimed to assess tissue-specific radiation doses associated with radon activity concentrations, that deposit similar dose levels as the annual natural radon exposure or radon gallery visits.

Methods: We exposed mice to defined radon concentrations, quantified the number of 53BP1 foci as a measure of induced DNA damage, and compared it with the number of foci induced by known doses of reference-type radiations. An image-based analysis of the 3-dimensional foci pattern provided information about the radiation type inflicting the DNA damage.

Results: A 1-hour exposure to 440 kBq/m^3 radon-induced DNA damage corresponding to a dose of ~10 mGy in the lung and ~3.3 mGy in the kidney, heart, and liver. A 1-hour exposure to 44 kBq/m^3 provided values consistent with a linear relationship between dose and radon concentration. Two-thirds of the dose in the lung was caused by α-particles. The dose in the kidney, heart, and liver and one-third of the dose in the lung likely resulted from β- and γ-rays.

Discussion: We found that radon exposures mainly lead to α-particle-induced DNA damage in the lung, consistent with the lung cancer risk obtained in epidemiologic studies. Our presented biodosimetric approach can be used to benchmark risk model calculations for radiation protection guidelines and can help to understand the therapeutic success of radon gallery treatments.

Corresponding author: Markus Löbrich, PhD; E-mail: lobrich@bio.tu-darmstadt.de

This work was supported by the Federal Ministry of Education and Research (02NUK017A/2NUK017E and 02NUK050A/02NUK050B) and by the Deutsche Forschungsgemeinschaft (GRK1657).

Disclosures: The authors declare they have no actual or potential competing financial interests.

Research data are stored in an institutional repository and will be shared on request to the corresponding author.

Supplementary material for this article can be found at https://doi.org/10.1016/j.ijrobp.2020.05.031.

Acknowledgments—We thank Monika Gawai for help with the experiments, Bettina Basso for analyzing tissue samples, and Franziska Papenfuß and Gerhard Kraft for many helpful discussions.

https://doi.org/10.1016/j.ijrobp.2020.05.031

Introduction

The radioactive decays of radon-222 (^{222}Rn) and its progenies contribute significantly to the natural radiation exposure worldwide. ^{222}Rn is formed within the uranium-radium decay series and represents the most stable radon isotope. As a noble gas with a half-life of 3.8 days, it can escape from cracks and crevices in the soil before it decays in its progenies that no longer possess noble gas properties. The radon concentration outdoors is relatively low, but radon can accumulate in housings,[1-3] where up to several kBq/m^3 are reached in certain areas and country-average activity concentrations typically range from 10 to 200 Bq/m^3. Epidemiologic studies demonstrated a direct link between lung cancer risk and radon concentration, consistent with a linear relationship without a threshold.[1,2,4-10]

Despite the established health risk, thousands of patients are treated worldwide in radon galleries to ameliorate chronic inflammatory joint diseases, diseases of the skin, or diseases of the respiratory tract.[11] A treatment series typically involves daily 1-hour stays for a period of about 10 to 12 days. During the visits, patients encounter radon activity concentrations of 50 to 100 kBq/m^3 and thus are exposed to 1000-fold higher radon levels than in their housings. Such exposures have been shown to induce long-term anti-inflammatory and pain-relieving effects, allowing patients to abstain from high-risk nonsteroidal anti-inflammatory drugs.[11-13] However, it is still controversially discussed as to whether the benefits justify the risks associated with radon exposure.

Detailed knowledge about the radiation types emitted during the decay chain of radon and how they potentially damage different organs is essential to understand the associated risks. Until the relatively stable ^{210}Pb isotope is formed, ^{222}Rn and its progenies ^{214}Po and ^{218}Po emit in total 3 α-particles, which have a range of a few centimeters in air and a few tens of μm in water. The other progenies ^{214}Bi and ^{214}Pb emit β-rays with a high range in air and a range of a few centimeters in water. Subsequently emitted γ-rays have a high range in air and water.[14] Owing to their different ranges, α-, β-, and γ-rays differentially damage the organs. It is additionally important to consider that α-particles deposit more energy in the damaged cells than β- and γ-rays. This is due to the high linear energy transfer (LET) of α-particles, meaning that multiple ionization events occur in close proximity along the path of an α-particle. The need to repair several damages in a confined space poses a severe problem for cells and has been suggested to account for the high biological effectiveness of α-particles, including their high carcinogenic effects.

The lung cancer risk obtained in epidemiologic studies is assessed per radon activity concentration (Bq/m^3) because the deposited dose (Gy) inside the lung cannot be directly measured.[1-10] Radiation protection authorities such as UNSCEAR and the ICRP currently estimate the dose either by comparison with other epidemiologic studies or from dosimetric and biokinetic models.[1-3,15,16] However, many variables used for such calculations are relatively unknown, leading to substantial uncertainties for estimates of the doses and associated risks.[17,18] Hence, there is a clear need to directly assess dose depositions from radon exposures.

A biological dosimetry approach can overcome these limitations by using a well-characterized cellular response as a readout for the deposited radiation dose such as the quantification of γH2AX or 53BP1 foci.[19-23] This technology detects single isolated DNA double-strand breaks (DSBs) arising linearly with the applied dose between a few mGy and several Gy, has exceptional sensitivity, and therefore can monitor the effects of very low radiation doses.[24,25] Foci analysis was applied by us and others to assess radiation doses encountered by humans during diagnostic medical procedures such as computer tomography examination.[26-29] Moreover, this technology was applied to different tissues[24,30] and different radiation qualities.[31,32] Not surprisingly, it is becoming the new gold standard for various biodosimetric applications.[20-22] Notwithstanding these benefits, γH2AX/53BP1 foci disappear within hours after irradiation due to repair, necessitating the need to control for the exposure time and for the time between radiation exposure and analysis.[21-23]

Here, we present an approach for assessing radiation doses associated with radon exposures based on 53BP1 foci biodosimetry in a mouse model system. We applied radon activity concentrations, that deposit similar dose levels as the annual natural radon exposure or radon gallery visits. We discuss potential mechanisms of how radon and its progenies might damage cells of various tissues and show further possibilities of how our approach can be used to benchmark risk model calculations. Our results have important implications for assessing the radiation risk and will help to understand the therapeutic success of radon gallery visits.

Material and Methods

Here, we provide information about the material and methods related to our work with mice and tissue. All information about our work with cultured cells to investigate the foci formation after irradiation with different dose rates can be found in the supplementary information (Appendix E2).

Irradiation of mice and sample preparation

Institutional and national guidelines for the care and use of laboratory animals were followed (see supplementary information, Appendix E1 for housing conditions and group sizes for experiments). Animal experiments were approved by the regional board of Darmstadt (V54-19c20/15-DA8/K5008). X-irradiation of mice was performed (without anesthesia) with an x-ray machine (X-Rad 320; Precision X-Ray) at 250 kV, 1 mA, and a dose rate of 100 mGy/min. Fe ion irradiation and radon exposure were

performed at the GSI in Darmstadt, Germany. Mice were exposed under anesthesia using isoflurane (1.5%, UniVet Porta, GROPPLER) to 4.2×10^4 Fe ions per cm^2 (1 GeV/u, 150 keV/μm) or without anesthesia to radon produced by a ^{226}Radium source in a specialized chamber.[33] Control mice were kept in the radiation control room during the experiments. The exposure time was 12 seconds for Fe ions (2, 1-second pulses separated by a 10-second pause) and 1 hour for radon (see supplementary information, Appendix E1 for details such as the equilibrium factor and the unattached/attached fraction of radon progenies). Organs were removed after cervical dislocation at 15 minutes, 1 hour, and 24 hours after IR (see supplementary information, Appendix E1 for fixation and preparation of tissue sections).

Foci counting, image acquisition, and statistical analysis

Counting of 53BP1 foci was typically performed in a blinded manner at a fluorescence microscope (Zeiss) using a 100× immersion objective. γH2AX signals were used to verify 53BP1 signals. Foci were quantified in ~500 cells on each of the 2 to 5 independently stained tissue sections evaluated for each mouse.

For foci area and intensity measurements and the classification in track and non-track foci, images were obtained with a confocal laser scanning microscope (Leica TCS SP5 II) using a 63× immersion objective and a pixel resolution of about $100 \times 100 \times 210$ nm^3 (see supplementary information, Appendix E1 for image acquisition settings). For the analysis of foci areas and intensities, the Z-plane with the highest signal intensity of each focus was selected, the foci boundaries were visually approximated, and the area and mean intensities were obtained (ImageJ, NIH). For the line plot analysis of γH2AX and 53BP1 signals, a maximum intensity projection of 4 to 10 Z-planes was used to visualize the entire track structure. Measurements were performed with Zen blue lite 2.6 software (Zeiss).

Statistical analysis was carried out by applying a one-sided *t* test with a significance level of 0.05. All details are provided in the supplementary information, Appendix E1. We performed all statistical tests with OriginPro 9.0G (OriginLabs).

Results

Evaluation of an appropriate model system

To assess radiation doses from radon exposures, we aimed to quantify the amount of DSBs by foci analysis. This approach meets all the requirements for a biodosimetric study. It is highly sensitive, and the number of foci scales linearly with the applied dose over many orders of magnitude.[25] The number of foci induced per unit dose is also independent of the dose rate during exposure (Fig. E1). Furthermore, the approach can be used to analyze foci, and therefore assess radiation doses, in a tissue-specific manner.[24,30,31,34,35]

We used mice as a model system which we and others previously used to study the effects of low-dose irradiations in vivo.[24,31,34,35] Because a single α-particle deposits a dose in the order of a few hundred mGy, exposure levels in the order of a few mGy or even less are expected to result in only a small fraction of damaged cells. To evaluate different tissues for their usefulness for our analysis, we investigated the interindividual variations in the level of spontaneously damaged cells between unirradiated mice and the response of the tissues to low doses of x-rays.

We isolated the lungs, kidneys, livers, and hearts of unirradiated and irradiated C57BL/6 mice, fixed the tissues, and stained tissue sections for the DSB marker 53BP1 at 15 minutes after irradiation (Fig. 1A), a time necessary for full foci formation.[23,31,36] Unirradiated mice showed similar average foci numbers per cell of about 0.04 and similar interindividual standard deviations of about 0.007 foci per cell for the 4 analyzed tissues (Fig. 1B). A whole-body x-ray dose of 10 mGy induced an additional number of 0.06 foci per cell similarly in all tissues (Fig. 1C), in agreement with previous data.[24] Thus, this model system is appropriate to assess radon exposures that are expected to induce foci numbers similar to, or even less than, a 10 mGy x-ray dose.

53BP1 foci formation after radon exposure

To expose mice to radon, we designed a special chamber[33] where radon-containing air obtained from a radium source was filtered to remove aerosols and filled into the chamber at a temperature of 20°C to 22°C and a humidity of 55% to 70% (for more details considering the exposure conditions see material and methods). We selected an exposure time of 1 hour and 2 radon activity concentrations of 44 and 440 kBq/m^3. The higher exposure of 440 kBq/m^3 was chosen because it physically corresponds to the situation of the natural radon concentration encountered over 1 year (assuming linearity between dose and both time and concentration, a 1-hour exposure to 440 kBq/m^3 equals an annual exposure time of 365×24 hours to 50 Bq/m^3, a concentration within the range of the natural radon concentration). The exposure of 440 kBq/m^3 also corresponds to the situation of gallery visits in which patients typically receive 1-hour exposures to 44 kBq/m^3 for 10 consecutive days. Note that we did not apply exposures for more than 1 hour because foci disappear due to DSB repair, precluding a reliable dose estimation.

Organs were isolated and fixed at 15 minutes after radon exposure, and tissue sections were stained for 53BP1. In contrast to the situation after x-rays, we often observed 53BP1 signals forming a track structure in cells of the lung that likely reflects the trajectory of an α-particle (Fig. 1D). We enumerated foci within such track structures individually whenever a substructure consisting of single foci was

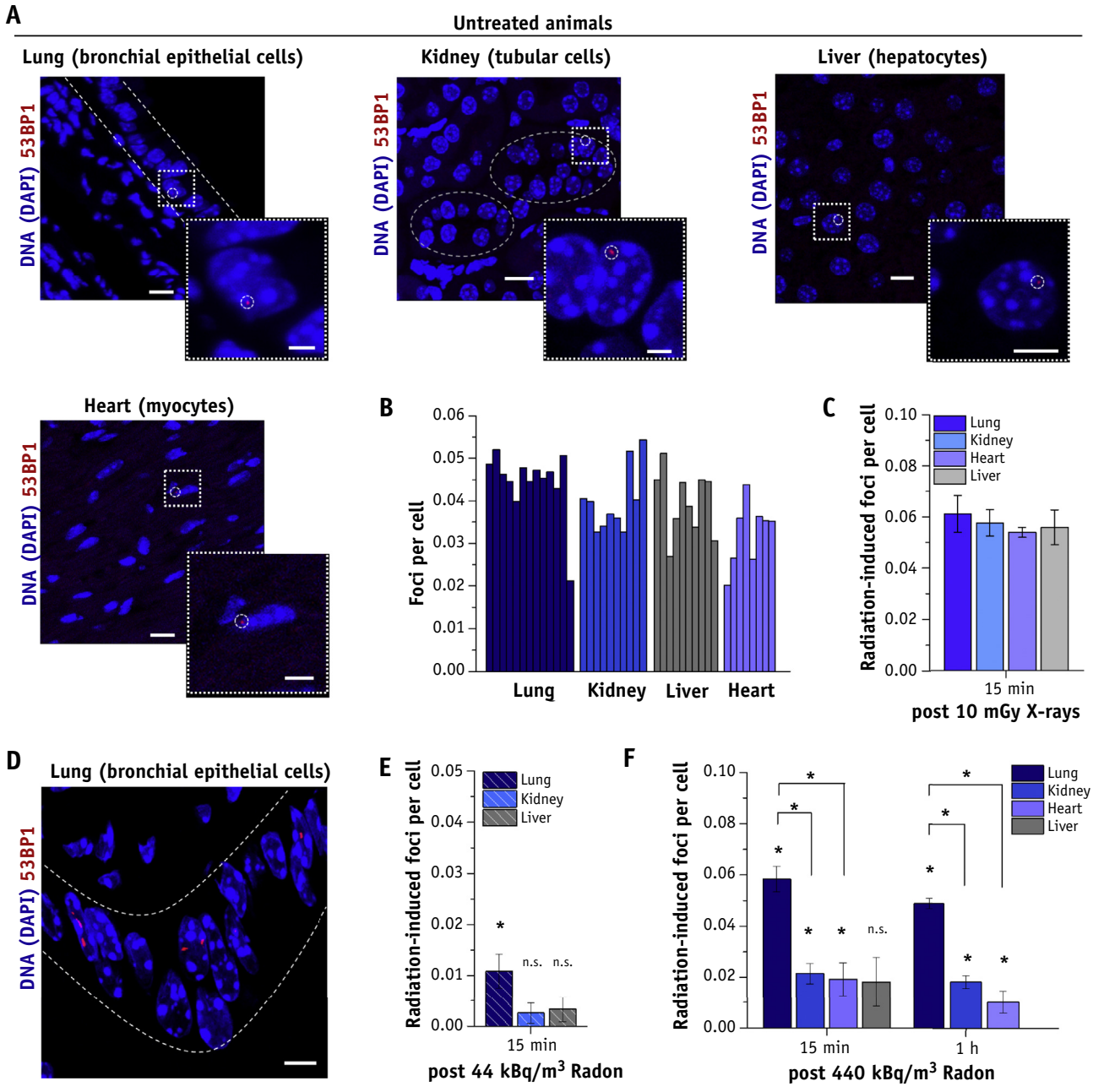

Fig. 1. Radiation-induced foci formation after radon exposure. (A) Immunofluorescence (IF) images of 53BP1 in various organs of unirradiated mice. The image headings specify the organs and cell types analyzed. The areas with the analyzed cells of the lung and the kidney are indicated with dashed lines. For the liver and the heart, all cells in the images were analyzed. For all organs, 1 representative cell is magnified. Scale bar: 10 µm in the overview images, 5 µm in the magnified images. (B) Quantification of 53BP1 foci in the lung, kidney, heart, and liver of unirradiated mice. (C) Radiation-induced 53BP1 foci in tissues of mice irradiated with 10 mGy x-rays. (D) IF image of 53BP1 in the lung of radon-exposed mice. Scale bar: 5 µm. The areas with the analyzed cells are indicated with dashed lines. (E, F) Radiation-induced 53BP1 foci in tissues of mice exposed to 44 kBq/m^3 (E) or 440 kBq/m^3 radon (F). Bars represent the average foci number of 1 (for panel B) or 3 mice (for panels C, E, and F), each evaluated by 2 to 3 experimenters. Foci were quantified in at least 2000 cells (for panel B) or 3000 to 4500 cells (for panels C, E, and F) for each tissue and mouse. Spontaneous foci quantified in tissues of unirradiated mice analyzed in parallel were subtracted (for panels C, E, and F). Error bars represent the standard error (SE) calculated by error propagation from the SE between the 3 irradiated mice and the SE of the corresponding untreated mice. Statistical significance was tested for irradiated versus unirradiated mice and between different tissues. $^*P < .05$. *Abbreviation:* n.s. = not significant.

observed. For mice exposed to 44 kBq/m^3, we observed a significant radon-induced increase in foci numbers for the lung (~0.011 foci per cell) but not for the kidney or the liver (Fig. 1E), suggesting that a single gallery visit can lead to detectable amounts of DSBs in the lung. For mice exposed to 440 kBq/m^3, we observed a radon-induced increase in foci numbers for all analyzed organs. The kidney, heart, and liver showed a similar increase (~0.018 foci per cell), and the lung exhibited 0.058 foci per cell (Fig. 1F). We also measured foci numbers at 1 hour postexposure and observed slightly lower values, indicating repair of DSBs and suggesting that no additional DSBs arose during the post-exposure period (Fig. 1F). This suggests that a condition physically corresponding to radon gallery visits and to the annual natural exposure to radon can lead to detectable amounts of DSBs not only in the lung but also in organs not directly in contact with the respiratory air. The higher dose deposition in the lung likely reflects the additional exposure to radon and its progenies adhering to inhaled aerosols. Of note, the foci levels in the lung of 0.011 (confidence interval: ±0.0064) and 0.058 (confidence interval: ±0.0099) for 44 and 440 kBq/m^3, respectively, are consistent with a linear relationship between dose and concentration. A linear regression analysis provided a slope of 1.33×10^{-4} foci per kBq/m^3 (standard deviation: $\pm 9.44 \times 10^{-6}$; R^2: 0.99), resulting in ~0.06 foci per cell for 440 kBq/m^3. The average of the foci numbers in the kidney, heart, and liver are also consistent with a linear relationship between dose and concentration ($0.41*10^{-4}$ foci per kBq/m^3; standard deviation: $\pm 1.38 \times 10^{-6}$; R^2: 0.99) and provide a value of ~0.02 foci per cell for 440 kBq/m^3. A linear relationship between foci numbers and radon concentration was also observed in other studies.[37,38]

53BP1 foci tracks after radon exposure

We considered the determined foci numbers after radon exposure unexpectedly high and investigated whether they represent the result of α-particle exposure. For this, we analyzed the 3-dimensional foci pattern and evaluated the fraction of foci arising within a track structure as a measure for α-particle-induced DSBs. We obtained high-resolution (confocal) microscopic images of 53BP1-stained lung tissue sections of unirradiated and radon-exposed mice. As negative and positive controls, we evaluated the fraction of foci arising within a track structure after x-rays, which are expected to generate only a few foci tracks by track-end electrons, and Fe ions, which are known to generate foci tracks. We defined foci as track foci if 2 or more foci formed a pearl-on-a-string-like structure in a single cell or if a single focus signal showed a very elongated form (Fig. 2A). The specificity and reliability of these signals were confirmed by colocalization studies with γH2AX signals (Fig. E2). The fraction of radiation-induced foci within foci tracks was calculated by dividing the number of foci in tracks in the irradiated samples minus the number of foci in tracks in unirradiated samples by the number of radiation-induced foci (Fig. E3A). We observed that ~70% of the radon-induced foci, ~15% of the x-ray-induced foci, and ~95% of the Fe ion-induced foci form tracks (Fig. 2B). The small but significant fraction of track foci after X-irradiation and the high number of tracks after Fe ions validated our foci classification. Thus, we suggest that α-particles, which are expected to induce foci within tracks, account for about two-thirds of the observed foci in the lung. The remaining one-third of the foci might arise from β- or γ-decays of radon progenies. Note that we were unable to reliably perform this analysis in other tissues due to the low number of radon-induced foci compared with background foci.

To substantiate the notion that the foci in lung tissues of radon-exposed mice represent, at least partly, α-particle-induced DSBs, we measured the total intensities of the 53BP1 foci (sum of all pixel intensities within a focus) in the same high-resolution images evaluated for the track structure analysis previously noted. Previous studies showed that this parameter differs between particle-induced and spontaneous or x-ray-induced foci.[31,32,39] Foci in X-irradiated samples showed only slightly higher signal intensity than foci in samples of unirradiated mice, which was further increased in radon-exposed samples (Fig. 2C). Importantly, track foci in the radon-exposed samples were substantially brighter and larger than nontrack foci in the same sample, similar to what was observed in samples after Fe ion irradiation (Fig. 2C; see also Fig. E3B,C). Thus, this evaluation shows that the track foci in radon-exposed samples show characteristics of particle-induced DSBs and hence confirms our analysis. The observation that track foci are on average brighter and larger than x-ray-induced foci[31,32,39] further suggests that 1 track focus might represent multiple DSBs.

Dose estimation after radon exposure

To estimate the physical doses associated with radon exposure, we compared the radon-induced foci levels with the foci levels induced by known doses of x-rays and Fe ions. We analyzed all samples with the same nonconfocal microscopic approach that was used for assessing foci levels in Figure 1 and also extended our analysis to a later time point to evaluate how the foci are repaired (24 hours after irradiation). Notably, a radon exposure for 1 hour at 440 kBq/m^3 induced about 0.06 foci per cell in the lung at 15 minutes post irradiation, similar to x-ray and Fe ion doses of 10 mGy. Foci levels in the kidney, heart, and liver, in contrast, were about 3-fold lower than after 10 mGy of x-rays and Fe ions (Fig. 3A). At 24 hours postirradiation, the foci level after radon exposure decreased due to repair to ~0.03, similar to the level after Fe ion irradiation but higher than what was observed after X-irradiation (Fig. 3B). The higher foci level after radon exposure and Fe ion irradiation compared with X-irradiation is consistent

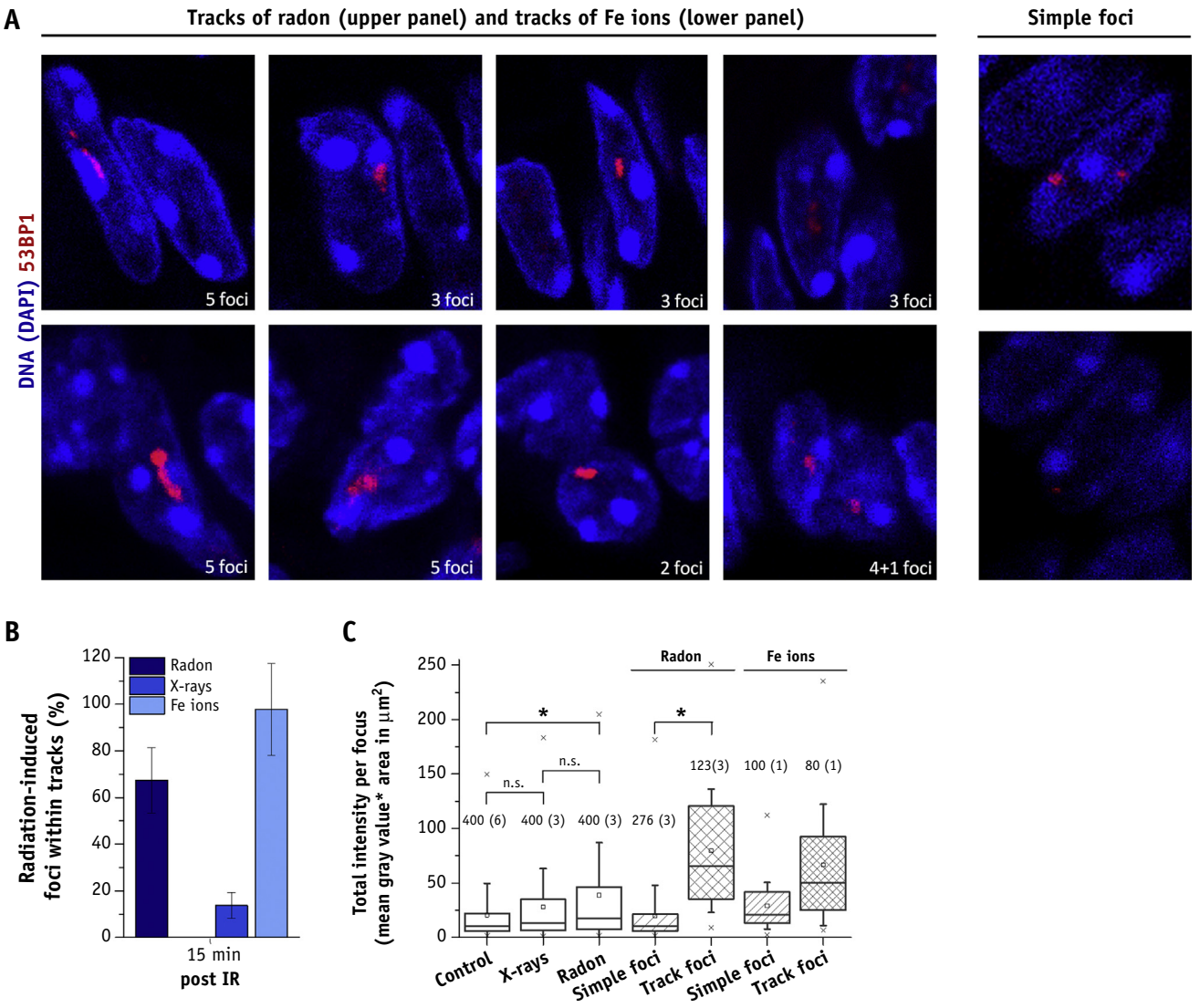

Fig. 2. Foci tracks after radon exposure. (A) Confocal IF images of 53BP1 signal classified either as track or simple foci in lung tissue. Each panel indicates the enumerated foci number per track. (B) Percentage of radiation-induced foci arising within tracks in the lung. For this analysis, foci in at least 1000 cells per mouse were classified in the confocal images (see Fig. E3A). Error bars represent the standard error between 3 mice. (C) 53BP1 foci intensities in the lung of mice at 15 minutes post-IR. The number of analyzed foci and mice is indicated for each condition. The whisker represents the standard deviation between foci intensities. The box encompasses 50% of the data points, the range between the "x" below and the "x" above the boxes 98% of the data points. Statistical significance was tested for the indicated conditions by comparing the mean values for the individual mice. $^{*}P < .05$. *Abbreviation:* n.s., not significant.

with our analysis that radon-induced foci show characteristics of Fe ion-induced foci, which are more difficult to repair than x-ray-induced DSBs.

The observation that the same radiation dose deposited by 2 radiation types with different ionization patterns (x-rays and Fe ions) induces similar foci numbers might seem surprising but is consistent with previous studies.[40,41] Thus, the finding that a radon exposure for 1 hour at 440 kBq/m^3 induces foci levels in lung tissues similar to a 10-mGy dose of x-rays or Fe ions provides strong evidence that this radon exposure corresponds to a dose deposition of approximately 10 mGy. This estimation is supported by the analysis of foci levels at 24 hours postirradiation in which Fe ion- and radon-induced foci levels were similar to each other and slightly higher than x-ray-induced foci levels. The 3-fold lower foci level in the kidney, heart, and liver likely corresponds to a 3-fold lower radiation dose because previous studies have shown that foci are induced linearly with dose in the range of a few mGy.[24,25]

Discussion

Radon exposure contributes substantially to the natural background irradiation and is estimated to account for about 3% to 14% of all lung cancer cases worldwide.[1-9]

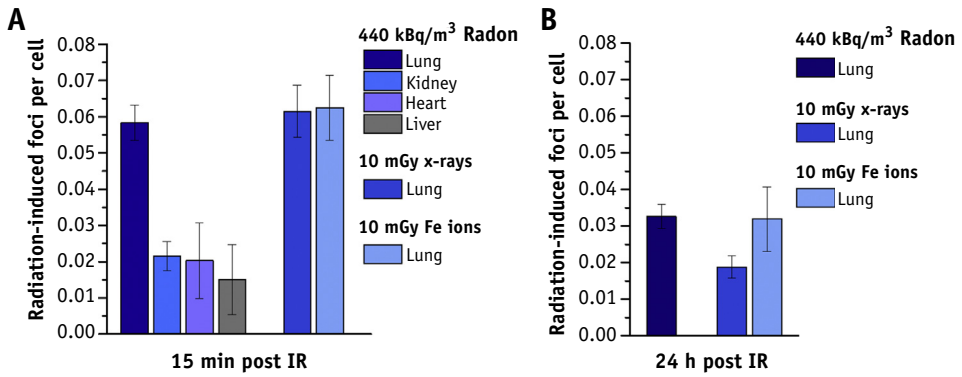

Fig. 3. Dose estimation after radon exposure. Radiation-induced 53BP1 foci at 15 minutes (A) or 24 hours (B) post-IR. Bars represent the average foci number of 3 mice (2 mice for the 24-hour data point after Fe ion exposure), each evaluated by 2 to 3 experimenters. Foci were quantified in 3000 to 4500 cells for each tissue and mouse. Spontaneous foci quantified in tissues of unirradiated mice analyzed in parallel were subtracted. Error bars represent the standard error (SE), calculated by error propagation from the SE between the 3 irradiated mice and the SE of the corresponding untreated mice. Data for radon and x-rays at 15 minutes post IR are shown in Figures 1C and 1F.

Moreover, radon is used at high concentrations as a therapeutic agent to treat patients with inflammatory diseases during gallery visits.[11,12] Estimates of radiation doses associated with radon exposures are based on model calculations, which inevitably have many uncertainties.[17,18] Additionally, it is largely unknown how radon exposure and the associated emissions of α-, β-, and γ-rays differentially affect different organs. Here, we aimed to estimate the doses by exposing mice to defined radon concentrations. We derived organ-specific dose estimates by comparing the level of DSBs inflicted by radon exposure with the level of DSBs caused by known doses of x-rays and high-energy Fe ions. We estimated that a 1-hour radon exposure at 440 kBq/m^3 deposits a radiation dose in the lung of exposed mice of ~10 mGy and a dose of ~3.3 mGy in the kidney, heart, and liver. A summary of the assessed dose levels in mice is provided in Figure 4. These doses may appear surprising, although other biodosimetric studies[38,42,43] also detected doses in the mGy range for extrapolated radon concentrations and exposure times similar to ours (see supplementary information, Appendix E3 for more information on these studies).

The dose in the kidney, heart, and liver is likely due to β-rays

It is important to know whether the dose deposition in organs other than the lung is caused by β- and/or γ-rays or by α-particles. For this, it needs to be considered that β-rays emitted during the radon decay chain from ^{214}Pb and ^{214}Bi have a range in water of about 0.5 to 2 cm and can reach from the surrounding air into the kidney, heart, and liver of mice. γ-rays have an even larger range and can similarly reach these organs. In contrast, α-particles have a range of a few tens of μm and can only damage these organs if they decay inside them. Because the solubility of radon in tissues is relatively low (0.025-2 kBq/kg),[44,45] the contribution of β- and γ-decays in the surrounding air to the dose in the kidney, heart, and liver is likely significantly larger than the dose contribution from α-decays inside these organs (see supplementary information, Appendix E3 for more details).

To find out whether the dose was caused by β- or γ-rays, it is important to consider that nearly the entire γ-ray energy from decays inside the chamber was deposited outside

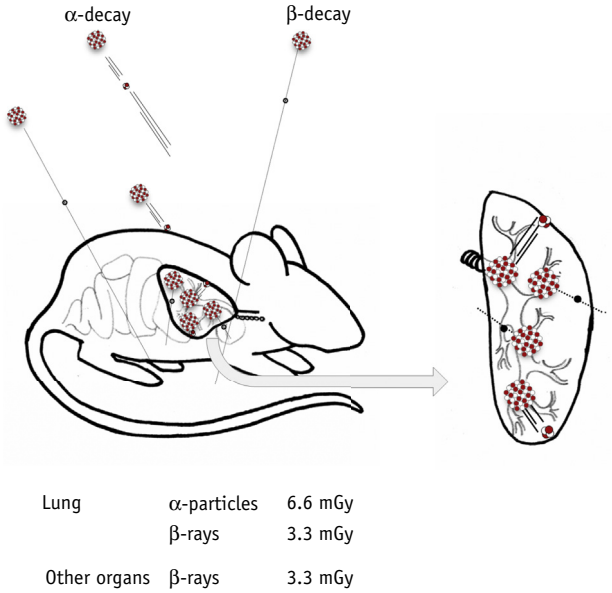

Fig. 4. Model for the dose contributions of α- and β-particles during radon exposure of mice. α-particles are depicted with triple-line solid and β-rays with single-line dotted trajectories. γ-rays and radon diffusion into tissues do not contribute significantly to the total dose deposition in the mouse and are not shown. The data summarizes the assessed dose levels in our mouse model for 440 kBq/m^3 radon.

the chamber and could not have damaged the mice. We, therefore, suggest that β- and not γ-rays caused the majority of the dose deposition in the kidney, heart, and liver. This interpretation is consistent with model calculations for phantom human bodies inside a standard room, which suggest very low γ-ray doses but a significant skin dose due to external β-irradiation.[46] Owing to differences in size between humans and mice, external β-irradiation will be able to reach the inner organs of the mice.

The additional dose in the lung is likely due to α-particles

Cells of the lung, similar to cells of the kidney, heart, and liver, will be damaged by β-rays arising in the air surrounding the mice. However, cells of the lung are in close contact with air in the bronchial tract and can also be reached by α-particles from the ^{222}Rn decay. Moreover, the radon progenies ^{214}Po and ^{218}Po are known to attach to aerosols that accumulate in the bronchial tract and emit α-particles.[1-3] The dose contribution due to aerosols likely depends on aerosol size, the equilibrium between radon and its progenies, and the unattached fraction of radon progenies, as well as on the breathing and mucous clearance rate. α-particles arising from radon and its progenies most likely cause the additional dose in mouse lung cells. Thus, we suggest that α-particles cause 2/3 of the dose in the lung, and β-rays from the surrounding air and aerosols in the lung account for 1/3 of the dose in the lung and the majority of the dose in all other organs. This interpretation is consistent with our observation that about 60% of the foci in lung cells arise within tracks. Of note, the additional dose received in lung cells compared with cells of the kidney, heart, and liver was about 6.6 mGy for a radon exposure of 440 kBq/m^3.

Limitations of our biodosimetric approach and further opportunities

Despite the benefits of the foci assay to assess dose levels associated with radon exposures, there are limitations. As already noted, foci disappear as a result of repair,[21-23] necessitating the need to control for the duration of the exposure and for the time between exposure and the assessment of foci. This limited the exposure time in our study to 1 hour and necessitated the application of high radon activity concentrations. The examination of lower radon concentrations would require longer exposure times to induce measurable foci numbers, which can only be achieved if foci loss during the exposure time is prevented. We envisage that the application of DSB repair inhibitors, eg, a DNA-PK inhibitor, might be 1 way to achieve this. Alternatively, repair-deficient mice, such as severe combined immunodeficient (SCID) mice carrying a DNA-PK mutation, are commercially available and could be used to enhance the sensitivity of the assay.

Foci analysis is ideally performed shortly after irradiation to prevent repair. If this cannot be achieved, it might be possible to deduce the number of induced foci from the measured value at later times. This, however, requires knowledge about the kinetics of foci loss, which depend on the radiation type and dose. In this context, it is noteworthy that foci induced by very low doses of x-rays (<10 mGy) persist for many days,[24,25] allowing a dose assessment even at long times after irradiation, although less reliably compared with an assessment at short times.

Another limitation is that α-particles and other high-LET radiation types induce foci in close proximity along their track, which cannot be easily resolved using conventional microscopy. This is indicated by the higher intensity and greater size of such foci[31,36,39] and likely leads to an underestimation of the actual foci number. This effect will not skew the dose assessment as long as the reference type radiation has a similar LET and level of foci underestimation. Nevertheless, high-resolution confocal microscopy in combination with a high-throughput scanning approach has the potential to efficiently image many cells with high resolution and will enhance the accuracy of the assay.

Conclusion

In summary, we have presented an approach to assess radiation doses in a living animal exposed to defined radon activity concentrations. Owing to the complex nature of radon exposure, involving different radiation types and different pathways of radioactive uptake, dose estimates from model calculations or physical measurements are typically restricted to specific aspects. In contrast, our holistic approach allowed us to monitor the entire spectrum of radon-induced dose deposition events in an organ-specific manner. We obtained the highest dose estimates in the lung due to inhaled α-particle emitters, consistent with the known lung cancer risk associated with radon exposures.

Further studies can easily be performed with other settings such as different radon or aerosol concentrations. The results of these studies can serve to benchmark model calculations currently used to assess doses and risks of radon exposures. Moreover, we envisage that the presented biodosimetric approach will be useful in further studies to assess doses in specific cell types that might help to explain the ameliorating effects of radon gallery visits.

References

1. United Nations Scientific Committee on the Effects of Atomic Radiation. UNSCEAR 2006 report vol II. Effects of ionizing radiation. Available at: https://www.unscear.org/unscear/en/publications/2006_2.html. Accessed June 10, 2020.
2. United Nations Scientific Committee on the Effects of Atomic Radiation. UNSCEAR 2000 report vol I. Sources and effects of ionizing radiation. Available at: https://www.unscear.org/unscear/en/publications/2000_1.html. Accessed July 7, 2020.

3. Paquet F, Bailey MR, Leggett RW, et al. ICRP publication 137: Occupational intakes of radionuclides: part 3. *Ann ICRP* 2017;46: 1-486.
4. Catelinois O, Rogel A, Laurier D, et al. Lung cancer attributable to indoor radon exposure in France: Impact of the risk models and uncertainty analysis. *Environ Health Perspect* 2006;114:1361-1366.
5. National Research Council (NRC). *Health Effects of Exposure to Radon: BEIR VI*. Washington, DC: National Academies Press; 1999.
6. Advisory Group on Ionising Radiation. Radon and public health. Documents of the Health Protection Agency. Radiation, chemicals and environmental hazards. 2009. Available at: https://www.gov.uk/government/publications/radon-and-public-health. Accessed July 7, 2020.
7. Darby S, Hill D, Auvinen A, et al. Radon in homes and risk of lung cancer: Collaborative analysis of individual data from 13 European case-control studies. *BMJ* 2005;330:223.
8. Brand KP, Zielinski JM, Krewski D. Residential radon in Canada: An uncertainty analysis of population and individual lung cancer risk. *Risk Anal* 2005;25:253-269.
9. Menzler S, Piller G, Gruson M, et al. Population attributable fraction for lung cancer due to residential radon in Switzerland and Germany. *Health Phys* 2008;95:179-189.
10. Kreuzer M, Fenske N, Schnelzer M, et al. Lung cancer risk at low radon exposure rates in German uranium miners. *Br J Cancer* 2015; 113:1367-1369.
11. Falkenbach A, Kovacs J, Franke A, et al. Radon therapy for the treatment of rheumatic diseases—Review and meta-analysis of controlled clinical trials. *Rheumatol Int* 2005;25:205-210.
12. Franke A, Franke T. Long-term benefits of radon spa therapy in rheumatic diseases: Results of the randomised, multi-centre IMuRa trial. *Rheumatol Int* 2013;33:2839-2850.
13. Ruhle PF, Wunderlich R, Deloch L, et al. Modulation of the peripheral immune system after low-dose radon spa therapy: Detailed longitudinal immune monitoring of patients within the RAD-ON01 study. *Autoimmunity* 2017;50:133-140.
14. Shapiro J. Radiation Protection, a Guide for Scientists, Regulators and Physicians. Cambridge, MA: Harvard University Press; 2002.
15. International Commission on Radiological Protection. ICRP publication 115. Lung cancer risk from radon and progeny and statement on radon. *Ann ICRP* 2010;40:1-64.
16. Muller WU, Giussani A, Ruhm W, et al. Current knowledge on radon risk: Implications for practical radiation protection? Radon workshop, 1/2 December 2015, Bonn, BMUB. *Radiat Environ Biophys* 2016;55:267-280.
17. Harley NH. Effect of residential radon decay product dose factor variability on reporting of dose. *Health Phys* 2018;114:398-407.
18. Hofmann W, Winkler-Heil R. From cellular doses to average lung dose. *Radiat Prot Dosimetry* 2015;167:49-54.
19. Anderson L, Henderson C, Adachi Y. Phosphorylation and rapid relocalization of 53BP1 to nuclear foci upon DNA damage. *Mol Cell Biol* 2001;21:1719-1729.
20. Barnard S, Ainsbury EA, Al-Hafidh J, et al. The first gamma-H2AX biodosimetry intercomparison exercise of the developing European biodosimetry network RENEB. *Radiat Prot Dosimetry* 2015;164: 265-270.
21. Kinner A, Wu W, Staudt C, et al. Gamma-H2AX in recognition and signaling of DNA double-strand breaks in the context of chromatin. *Nucleic Acids Res* 2008;36:5678-5694.
22. Lobrich M, Shibata A, Beucher A, et al. GammaH2AX foci analysis for monitoring DNA double-strand break repair: Strengths, limitations and optimization. *Cell Cycle* 2010;9:662-669.
23. Rogakou EP, Pilch DR, Orr AH, et al. DNA double-stranded breaks induce histone H2AX phosphorylation on serine 139. *J Biol Chem* 1998;273:5858-5868.
24. Grudzenski S, Raths A, Conrad S, et al. Inducible response required for repair of low-dose radiation damage in human fibroblasts. *Proc Natl Acad Sci U S A* 2010;107:14205-14210.
25. Rothkamm K, Lobrich M. Evidence for a lack of DNA double-strand break repair in human cells exposed to very low x-ray doses. *Proc Natl Acad Sci U S A* 2003;100:5057-5062.
26. Grudzenski S, Kuefner MA, Heckmann MB, et al. Contrast medium-enhanced radiation damage caused by CT examinations. *Radiology* 2009;253:706-714.
27. Kuefner MA, Grudzenski S, Hamann J, et al. Effect of CT scan protocols on x-ray-induced DNA double-strand breaks in blood lymphocytes of patients undergoing coronary CT angiography. *Eur Radiol* 2010;20:2917-2924.
28. Lobrich M, Rief N, Kuhne M, et al. In vivo formation and repair of DNA double-strand breaks after computed tomography examinations. *Proc Natl Acad Sci U S A* 2005;102:8984-8989.
29. Rothkamm K, Balroop S, Shekhdar J, et al. Leukocyte DNA damage after multi-detector row CT: A quantitative biomarker of low-level radiation exposure. *Radiology* 2007;242:244-251.
30. Bonner WM, Redon CE, Dickey JS, et al. GammaH2AX and cancer. *Nat Rev Cancer* 2008;8:957-967.
31. Mirsch J, Tommasino F, Frohns A, et al. Direct measurement of the 3-dimensional DNA lesion distribution induced by energetic charged particles in a mouse model tissue. *Proc Natl Acad Sci U S A* 2015;112: 12396-12401.
32. Nakajima NI, Brunton H, Watanabe R, et al. Visualisation of γH2AX foci caused by heavy ion particle traversal; distinction between core track versus non-track damage. *PloS One* 2013;8:e70107.
33. Maier A, van Beek P, Hellmund J, et al. Experimental setup for radon exposure and first diffusion studies using gamma spectroscopy. *Nucl Instru Methods Phys Res B* 2015;362:187-193.
34. Barazzuol L, Jeggo PA. In vivo sensitivity of the embryonic and adult neural stem cell compartments to low-dose radiation. *J Radiat Res* 2016;57:i2-i10.
35. Flockerzi E, Schanz S, Rube CE. Even low doses of radiation lead to DNA damage accumulation in lung tissue according to the genetically-defined DNA repair capacity. *Radiother Oncol* 2014;111:212-218.
36. Costes SV, Chiolo I, Pluth JM, et al. Spatiotemporal characterization of ionizing radiation induced DNA damage foci and their relation to chromatin organization. *Mutat Res* 2010;704:78-87.
37. Ding D, Zhang Y, Wang J, et al. γ-H2AX/53BP1/pKAP-1 foci and their linear tracks induced by in vitro exposure to radon and its progeny in human peripheral blood lymphocytes. *Sci Rep* 2016;6:38295.
38. Wang J, He L, Fan D, et al. Establishment of a γ-H2AX foci-based assay to determine biological dose of radon to red bone marrow in rats. *Sci Rep* 2016;6:30018.
39. Neumaier T, Swenson J, Pham C, et al. Evidence for formation of DNA repair centers and dose-response nonlinearity in human cells. *Proc Natl Acad Sci U S A* 2012;109:443-448.
40. Rydberg B, Heilbronn L, Holley WR, et al. Spatial distribution and yield of DNA double-strand breaks induced by 3-7 MeV helium ions in human fibroblasts. *Radiat Res* 2002;158:32-42.
41. Lobrich M, Cooper PK, Rydberg B. Non-random distribution of DNA double-strand breaks induced by particle irradiation. *Int J Radiat Biol* 1996;70:493-503.
42. Thomassen DG, Newton GJ, Guilmette RA, et al. A biodosimetric approach for estimating radiation dose to the respiratory epithelium from inhaled radon progeny. *Radiat Protect Dosimetry* 1991;38:65-71.
43. Johnson NF, Newton GJ. Estimation of the dose of radon progeny to the peripheral lung and the effect of exposure to radon progeny on the alveolar macrophage. *Radiat Res* 1994;139:163-169.
44. Ishimori Y, Tanaka H, Sakoda A, et al. Measurements of radon activity concentration in mouse tissues and organs. *Radiat Environ Biophys* 2017;56:161-165.
45. Sanjon EP, Maier A, Hinrichs A, et al. A combined experimental and theoretical study of radon solubility in fat and water. *Sci Rep* 2019;9:10768.
46. Markovic VM, Krstic D, Nikezic D, et al. Doses from radon progeny as a source of external beta and gamma radiation. *Radiat Environ Biophys* 2012;51:391-397.